Breakdown of ion-polarization-correspondence and born effective charges: Algebraic formulas of accurate polarization under field

Yukio Watanabe*
Kyushu University, Fukuoka, Japan

(Received 20 June 2020; accepted 11 September 2020; published 8 October 2020)

Polarization, especially of ferroelectrics FEs, is conventionally described by ion positions, e.g., by Born effective charges, where the complete entanglement of electron polarization with that of ions is implicitly assumed. We find that such descriptions or Born effective charge polarization-type approaches break down partially in the presence of high field, owing to the partial disentanglement of electrons with ions. To overcome this, we propose a correction (non-Born effective charge polarization) that calculates both macroscopic and unit-cell-by-unit-cell total polarization accurately. The accuracy of this method is demonstrated in prototypical situations of depolarization field E_d that exists in finite-size or inhomogeneous insulating FEs: paraelectric/FE, FE capacitors, and FE/vacuum. Here, FE/vacuum are shown to be electrically identical to encountering domains. This method provides simple algebraic formulas to calculate total polarization P_S and E_d using conventionally estimated polarizations that are obtained from local ion positions. Therefore, it can be easily used in experimental estimations of P_S and E_d, including 3D cases. For example, this method reveals that P_S varies across ferroelectric/insulator far less than the conventional estimate, which explains substantially reduced E_d and the absence of metallicity. In addition, vortexlike domains are discussed in view of E_d. The partial disentanglement of ion and electron polarization would imply limitation of Ginzburg-Landau framework of ferroelectrics under high field.

DOI: 10.1103/PhysRevMaterials.4.104405

I. INTRODUCTION

Ferroelectrics (FEs) have reversible spontaneous polarization P_S that is useful in numerous applications, for which a good insulator with a wide bandgap Eg is desired to apply external electric field E_{ext}. In real, i.e., finite-size FE, the depolarization electric field E_d exists in FEs even for $E_{ext} = 0$; E_d emerges by the existence of surfaces, interfaces, and inhomogeneity in the direction of P_S [Figs. 1(a)–1(c)]. E_d is considered essential for domain configurations [1–6], and the properties and existence of FEs [7–10]. For example, a simple Kittel model based on E_d [1] shows nanometer-scale vortexlike P_S patterns and nanodomains [6].

The emergence of the spontaneous polarization in standard FEs is described by the disappearance of inversion-symmetric ion positions. Accordingly, the phase transitions and properties of FEs are explained by the polar distortions of ion positions u [2,11–14] and their dynamics, i.e., polar soft-mode phonons. That is, the polar distortions of ion positions are equated with the spontaneous polarization, as shown by Ginzburg-Landau theory as a linear relationship between polarization and lattice strain η, e.g., $\eta = QP_S^2$ for stress-free case, where Q is constant [15] [Fig. 1(d)].

For the understanding of FEs, especially nanometer-scale FEs, atomic-scale understanding of polarization and E_d is indispensable. Standard experimental atomic-scale estimations of spontaneous polarization are based on local ion positions or distortion u [11,12] measured by x-ray diffraction or transmission electron microscopy (TEM). These estimations are performed also for $E_d \neq 0$ and $E_{ext} \neq 0$ [2–5,7,8] and basically the same as those using phonon modes with Born effective charges Z^* [13] that are defined at *macroscopic electric field* $E = 0$.

These local ion-position based estimations are used also in *ab initio* calculations; for example, the surface of freestanding FEs and head-to-head/tail-to-tail (HH-TT) domains possess metallic bands owing to E_d, when $P_S \perp$ surfaces or $P_S \perp$ boundaries [10,16–19]. In these cases, empirical formulas based on ion positions or Born effective charges are used [10,19].

The present paper suggests the polarization that has been missing in these conventional estimates. In case of partly metallic FE slabs [Fig. 1(e)], E_d originates from surfaces or domain boundaries, which are absent in the extracted (copied) bulk unit-cell [Fig. 1(f)] that has the same ion positions of the unit-cell in the slab [Fig. 1(e)] (Table I). Consequently, E_d is absent in the copied bulk unit-cell, although the ion positions are exactly the same as those in the slab and contain the ion distortion u due to E_d. Because electrons move with ions, the polarization of electrons in the slab is partly included in the polarization of this extracted bulk unit-cell $P_S^{\text{iso-bulk}}$, whereas the polarization of ions in the slab is completely included in $P_S^{\text{iso-bulk}}$. $P_S^{\text{iso-bulk}}$ corresponds to the polarization described by conventional estimates based on local ion-positions such as Born effective charge $\Sigma Z^* u$ [distortion u depends on E: $u(E)$].

Because of the similarity of the physics or spirit, we relate $P_S^{\text{iso-bulk}}$ with Born effective charges, although P_S by Born

*watanabe@phys.kyushu-u.ac.jp

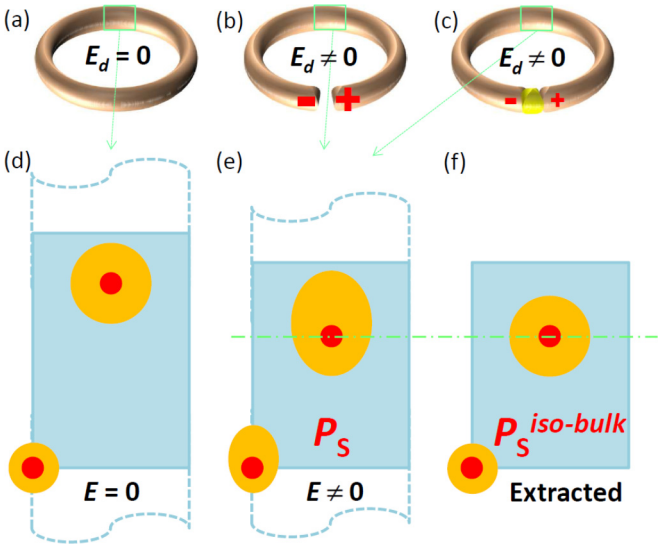

FIG. 1. Images of bulk and real FEs [(a)–(c)], the corresponding unit-cells [(d)–(f)] explaining extracted bulk unit-cell, $P_S^{\text{iso-bulk}}$ and P_{el}^{Exra}. (a) bulk, i.e., infinite-size FE. (b), (c) real, i.e., finite-size FEs: FE/vacuum (b) and FE heterostructures (c), where E_d emerges owing to the imperfect screening of polarization charges. (d)–(f) FE unit-cells showing ions (red) and electron clouds (orange): (d) short-circuit slab, (e) open-circuit slab, and (f) bulk having the same ion positions as (e).

effective charges may deviate from a Berry phase P_S even for $E = 0$ [20] and, hence, from $P_S^{\text{iso-bulk}}$. However, P_S estimated by an optimized $Z^*(u)u$ could agree almost perfectly with Berry phase P_S for a wide range, while the difference between P_S's estimated with Berry phase using different exchange correlation functionals was visible (Appendix). Therefore, in general, ideal Born effective charges would be able to agree with the exact P_S by optimizing Z^* for each *specific FE* and including the exact dependence of Z^* on u, stress σ, and specific atomic environments such as defects. To express the physics, $P_S^{\text{iso-bulk}}$ is identified with Born polarization estimated by such ideal Born effective charges ($P_S^{\text{iso-bulk}}{}_{\text{BornI}}$) that are optimized for a specific FE; $P_S^{\text{iso-bulk}}{}_{\text{BornI}}$ agrees perfectly with P_S estimated with ideal Berry phase $P_S^{\text{iso-bulk}}{}_{\text{Berry}}$.

Nonetheless, $P_S^{\text{iso-bulk}}$ or $P_S^{\text{iso-bulk}}{}_{\text{BornI}}$ is considered to overlook the possibility that electrons move partly freely from ions; even when ion positions are the same, the polarization of electrons or atomic polarization [21] may be different for $E = 0$ and $E \neq 0$ [Figs. 1(e) and 1(f)]. Hence, the total polarization for $E \neq 0$ is considered as $P_S^{\text{iso-bulk}} + P_{el}^{Extra}$, where $P_S^{\text{iso-bulk}}(u)$ is the polarization of ion and electrons for $E = 0$ at $u = u(E)$ (u is attained by E) and $P_{el}^{Extra} = (\varepsilon_{Extra}^{el} - 1)\varepsilon_0 E$ is an extra polarization by E (ε_{el}^{Extra}: permittivity of electrons for extra polarization). The validity of these postulates shall be explained more in Sec. III and proved in Sec. IV.

When this inference is correct, this extra polarization P_{el}^{Exra} cannot be expressed by the improvements of $P_S^{\text{iso-bulk}}{}_{\text{Berry}}$ or $P_S^{\text{iso-bulk}}{}_{\text{BornI}}$ that include several effects such as the dependence of Z^* on u, σ, and E [22] and the rescaling [19,23]; Total polarization is $P_S^{\text{iso-bulk}} + (\varepsilon_{el}^{Extra} - 1)\varepsilon_0 E$, where we call P_{el}^{Extra} non-Born polarization considering ideal Born effective charges: $P_S^{\text{iso-bulk}}{}_{\text{BornI}} = P_S^{\text{iso-bulk}}$. Consequently, P_{el}^{Exra} is not included in the molecular dynamics (MD) simulations based on effective Hamiltonian [9,24] and classical (non-*ab initio*) MD simulations [25]. Similarly, the accurate experimental estimation of polarization from local ion positions or u [2–5,7,8,11,12] is $P_S^{\text{iso-bulk}}$, and, therefore, does not contain P_{el}^{Exra}.

We have found that P_{el}^{Exra} often reduces E_d drastically and propose a method to calculate this polarization, where ε_{el}^{Extra} can be sufficiently approximated by the *static* permittivity of electrons ε^{el}. For paraelectric under low E, P_{el}^{Exra} may be corrected by rescaling $P_S = C_R P_S^{\text{iso-bulk}}$ [19,23], where $C_R = (1 + (\varepsilon^{el} - 1)/\chi^{ion}) \approx 0.90$ and χ^{ion} is the susceptibility due to ions. This formula is equivalent to rescaling of Born effective charge Z^{*R}: $Z^{*R} = C_R Z^*$. On the contrary, the present extra polarization P_{el}^{Exra} is based on the polarization independent of u's as expressed in the second term in $P_S^{\text{iso-bulk}} + (\varepsilon_{el}^{Extra} - 1)\varepsilon_0 E$; consequently, E_d is not determined by local $P_S^{\text{iso-bulk}}$ as in the rescaling [23] but is determined by global distribution of $P_S^{\text{iso-bulk}}$ as in the equations in Sec. III. Also P_{el}^{Exra} is different from the E-dependence $\Sigma[Z^* + \Delta Z^*(E)]u$ proposed for semiconductors [22].

Using the consistencies of conventionally estimated polarization $P_S^{\text{iso-bulk}}$ [11–15], we propose a method that calculates P_{el}^{Exra} and total polarization, including three-dimensional (3D) cases. This method can also be performed only with global ion position data and, hence, is usable in experimental studies such as those using TEM [2–5,7,8]. We demonstrate the necessity and accuracy of non-Born polarization P_{el}^{Exra} in prototypical situations of E_d: FE/vacuum, paraelectric/FE, and

TABLE I. Lattice constants and ion positions of tetragonal $BaTiO_3$ exemplarily explaining the procedure to obtain the extracted (copied) bulk unit-cell for $P_S^{\text{iso-bulk}}$ [Fig. 1(f)] that has the same ion positions of the unit-cell in the slab [Fig. 1(e)]. This example corresponds to BTO in BTO(7PBE + U)/STO in Fig. 4, and ion positions are shown in fractional coordinates. The second row shows the lattice constants and ion positions of bulk $BaTiO_3$. The third and fourth rows show the lattice constants and ion positions of BTO unit-cell in the center of BTO layers in the BTO/STO slab, where the fractional coordinates are with respect to the lattice constants of slab and the unit-cell, respectively. The fifth row shows the lattice constants and ion positions of BTO unit-cell of extracted unit-cell, which is identical with the fourth row.

Fractional coordinates in a and c	a (Å)	z_{bottomBa} (0,0,z_{Ba})	z_{topBa} (0,0,z_{Ba})	c (Å)	z_{Ti} (0.5,0.5,z_{Ti})	z_{O2} (0,0.5,z_{Ti}) (0.5,0,z_{Ti})	z_{O1} (0.5,0.5,z_{Ti})
Bulk	3.979	0	1	4.069	0.5141	0.4837	−0.0301
Slab center	3.947	0.29749	0.38245	47.920	0.34118	0.33914	0.29564
Slab center	3.947	0	1	4.071	0.5142	0.4903	−0.0218
Copied bulk	3.947	0	1	4.071	0.5142	0.4903	−0.0218

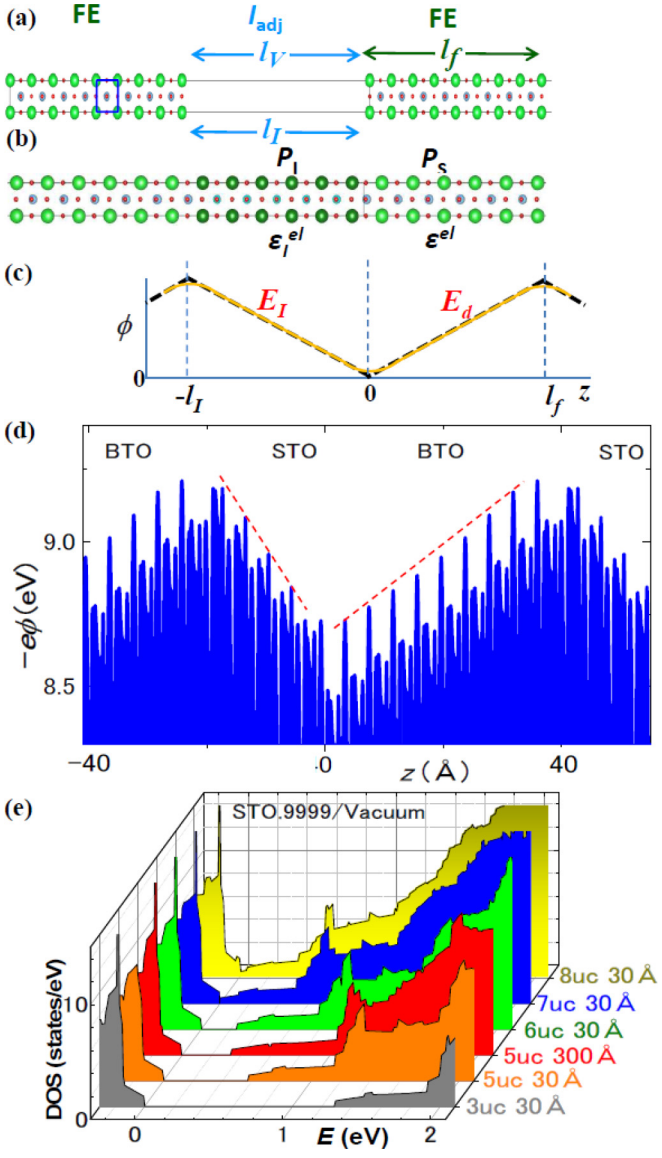

FIG. 2. Atomic model of (a) FE/vacuum and (b) FE/I_{adj} superlattice, and (c) corresponding macroscopic potential ϕ. (d) Example of the estimation of *ab initio* E_d ($E_d^{ab\ initio}$) from the highest planar averaged atomic potential ϕ by the *ab initio* calculation of 10-unit-cell BTO/5-unit-cell STO. (e) DOS of STO.9999/vacuum, where l_f in the unit of unit-cells and l_V in Å are shown on the right.

FE capacitors [Figs. 1(b), 1(c), and 2]. Here, FE/vacuum can represent HH-TT domains. In view of reduced E_d, the vortex domains [3–5,9,24,25] are discussed in comparison with flux closures [26–28].

II. TECHNICAL DETAILS

To calculate P_S *ab initio*, we used insulating FE slabs consisting of $SrTiO_3$ (STO) and archetypical FE $BaTiO_3$ (BTO). For the achievement of the insulativity of FE, which was necessary for the *ab initio* calculation of P_S of a whole slab, FE in FE/vacuum [Fig. 2(a)] required a small P_S and a large Eg (Appendix). These requirements were achieved by SrO-terminated STO's (P4mm) having a-axis lattice constant 0.5% longer and 0.01% shorter than that of the theoretical cubic phase [29]. We call them STO1.005 and STO.9999, respectively, of which lattice-constants a and c, and P_S are 3.902 Å, 3.896 Å, 3.56 μC/cm^2, 3.897 Å, 3.898 Å, and 6.15 μC/cm^2, respectively [29]. For FE/vacuum, geometries were not relaxed, because otherwise FE disappears (Appendix); The FE unit-cells in each slab retained the ion positions of STO1.005 or STO.9999. Therefore, $P_S^{iso\text{-}bulk}$ of any unit-cell was the same as the above bulk value: 3.56 μC/cm^2 or 6.15 μC/cm^2. These calculations were only for the examination of P_{el}^{Exra} and ε_{el}^{Extra} and were not intended to explain experiments.

BTO/STO superlattices were used as FE/insulator heterostructures [Fig. 2(b)]. All the calculated forces were <1 meV/Å after geometry relaxation. In the calculation of BTO capacitor structures with PBEsol, a standard electrode material $SrRuO_3$ was 5 unit-cell thick $\sim$20 Å. The a-lattice constant of BTO/$SrRuO_3$ was fixed at the theoretical a of cubic STO, and all other ion positions were relaxed, which corresponds to the epitaxial films on STO substrates. The surfaces of the BTO and $SrRuO_3$ were TiO_2 and SrO, respectively.

In the remainder, I_{adj} stands for both vacuum in FE/vacuum and insulator in FE/insulator, and P_I and E_I stand for the polarization and the depolarization field in I_{adj}, respectively [Fig. 2(a)]. $P_S^{iso\text{-}bulk}$ and $P_I^{iso\text{-}bulk}$ denote the polarizations of the extracted unit-cells from FE and I_{adj}, respectively, which can be calculated from local ion positions. An example of the extracted unit-cell is indicated by a blue small rectangle in Fig. 2(a). The permittivity's of electrons and the thickness of FE and I_{adj} are denoted by ε^{el}, ε_I^{el}, l_f, and l_I ($= l_V$ for I_{adj} = vacuum), respectively, and the length of the slab l_{SC} is $l_f + l_I$. The periodic behavior of the potential in Fig. 2(c) suggests $l_f E_d = -l_I E_I$. *Ab initio* E_d ($E_d^{ab\ initio}$) was obtained from the envelope of the peak tops of atomic potential, where the dashed red lines in Fig. 2(d) are the example of this envelope (also in Appendix).

In these calculations, no dipole correction was applied, as usual for the studies of FE/I_{adj} superlattices and FE capacitors (The appropriateness for FE/vacuum is explained in Appendix). These *ab initio* calculations rigorously correspond to the macroscopic model in Fig. 2(c), which is sufficient for the present paper. The correctness of no dipole correction is evident in the excellent agreements between $E_d^{ab\ initio}$ and analytical E_d [30] and between *ab initio* and analytical P_S (Sec. IV). These results also explain quantitatively the decrease of E_d with l_f and the emergence of metallicity in Fig. 2(e).

In the *ab initio* calculations with VASP [31], the projector augmented wave (PAW) method [32] was used with PBEsol functional [33], a Monkhorst-Pack [34] mesh of $8 \times 8 \times 2$, and with an energy cutoff of 650 eV. *Ab initio* P_S and $P_S^{iso\text{-}bulk}$ were obtained by Berry phase calculations [35]. In case of FE/vacuum, the dipole moment of a whole FE/vacuum slab was calculated with Berry phase, and P_S was obtained by dividing this dipole moment by the volume of FE part ($a \times a \times l_f$), which we call a "rigorously calculated P_S of the slab." The calculations of BTO/STO superlattices were examined also with PBE functional [36] with Hubbard U [37] (PBE+U: U on Ti 3d and O 2p). Optical permittivity of bulk STO and BTO was calculated with ex-

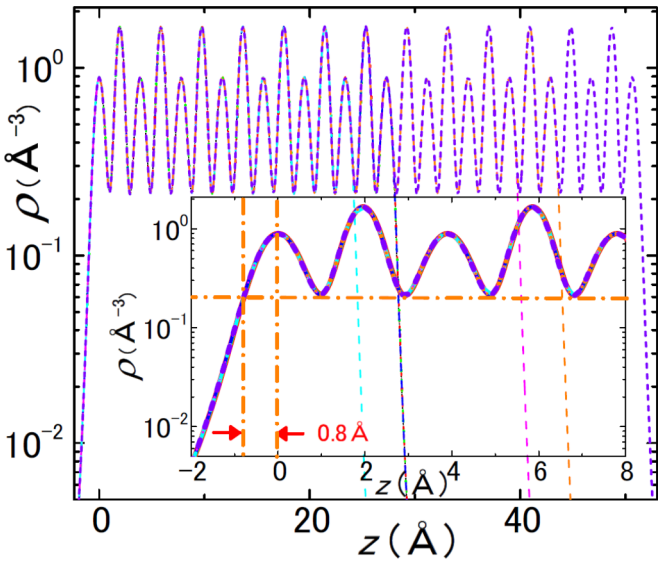

FIG. 3. Planar averaged electron density ρ for estimating the FE thickness l_f. All the eight ρ's behave the same near the surface, supporting the use of the same smearing length ∼0.8 Å for different slabs. Inset shows the enlarged view near the surface.

act diagonalization and random phase approximation (RPA). *E*g's are calculated with PBEsol, PBE+U, and a hybrid functional HSEsol [38], where PBEsol is known to underestimate *E*g's typically by 30%, while HSEsol yields appropriate values [39].

In the present calculations of FE/vacuum, it is important how to define the location of FE surface, i.e., l_f. Therefore, l_f was estimated from the planer averaged electron density ρ profiles in Fig. 3, which displays that all the ρ profiles of 8 different slabs exhibit the same behaviors near the surface. This is more evident in the enlarged view at $z \approx 0$, where all the ρ profiles of eight different slabs overlap. The ρ peaks at the right and left end ($z = 0$) correspond to the BaO of the top and bottom surface, respectively. ρ at $z = -0.8$ Å is same as the minimum ρ of inner part in all the $\rho - z$ curves. This means that the region of $z = 0 \sim -0.8$ Å should be considered as a part of FE, and l_f is the distance of top and bottom outermost ion (Ba) position plus 2×0.8 Å. As for l_I, $l_I = l_{\rm SC} - l_f$.

In the calculation of BTO/STO, l_f was defined as the distance between the top and bottom Ti ions of BTO, and $l_I = l_{\rm SC} - l_f$. In the calculation of BTO/$SrRuO_3$ capacitor structures, the effective l_f ($l_f^{\rm eff}$) was $l_{\rm T-B} - {\rm uc}_{\rm BTO}$, where $l_{\rm T-B}$ is the distance between top and bottom Ti (top and bottom of BTO are TiO_2's) and ${\rm uc}_{\rm BTO}$ is the length of a BTO unit-cell. The results with $l_f^{\rm eff} = l_{\rm T-B} - 1.5\ {\rm uc}_{\rm BTO}$ were almost the same.

III. METHODS

Section I postulated $P_{\rm S} = P_{\rm S}^{\rm iso\text{-}bulk} + P_{\rm el}^{\rm Exra}$ with $P_{\rm el}^{\rm Exra} = (\varepsilon_{\rm el}^{\rm Extra} - 1)\varepsilon_0 E$, of which technical details are explained in Fig. 1, Table I, and the Appendix. The background of the formulas are as follows. Within Born-Oppenheimer adiabatic approximation, electron distribution ρ is considered to depend on a total field: atomic fields from ions ($E_{\rm ion}^a$), of which macroscopic average is zero, and macroscopic field E, e.g., E_d. E displaces ions ($u(E)$), yielding ion polarization $P_{\rm ion}(u)$. Because of the coupling to $E_{\rm ion}^a(u)$ and E, $\rho(E_{\rm ion}^a(u), E) = \rho(u, E)$, which yields electron polarization $P_e(\rho) = P_e(\rho(u, E)) = P_e(u, E)$. This expression $P_e(u, E)$ is needed, because in general cases electrons and each ion are governed by their own different mechanics.

For a weak E, $P_{\rm S} = P_{\rm ion}(u) + P_e(u, 0)$ can be rigorously expressed by ideal Born effective charges $P_{\rm S} = \Sigma Z^* u$, thanks to the robust interactions between ions and electrons ($E_{\rm ion}^a$). As the last paragraph indicates, such complete entanglement of P_e with u and, hence, ion polarization $P_{\rm ion}$ is approximate, when E is nonnegligible in comparison with $E_{\rm ion}^a$. That is, the straightforward expression $P_{\rm S} = P_{\rm ion}(u) + P_e(\rho)$ is more appropriate than $P_{\rm S} = \Sigma Z^* u$.

Therefore, $P_{\rm S} = P_{\rm ion}(u) + P_e(\rho) = P_{\rm ion}(u) + P_e(u, E) \approx P_{\rm ion}(u) + P_e(u, 0) + \Delta P_e E = P_{\rm S}^{\rm iso\text{-}bulk} + P_{\rm el}^{\rm Exra}$, where $P_{\rm S}^{\rm iso\text{-}bulk} \equiv P_{\rm ion}(u(E)) + P_e(u(E), 0)$, $P_{\rm el}^{\rm Exra} \equiv \Delta P_e E$, and quasi-equality is for $E \ll E_{\rm ion}^a$. Below, $\varepsilon_{\rm el}^{\rm Extra}$'s are approximated by the static permittivity of electrons $\varepsilon^{\rm el}$, as explained by the end of Sec. III.

The 1D-polarizations below denote the components perpendicular to the surfaces and interfaces (1D refers to the case where properties change only along one coordinate as in Fig. 2). Therefore, the polarizations below such as $P_{\rm S}$, P_I, $P_{\rm S}^{\rm iso\text{-}bulk}$, and $P_I^{\rm iso\text{-}bulk}$ should be multiplied by $\cos\theta$ (θ: incidence angle), when the total polarizations are oblique to the surfaces and interfaces (Appendix).

A. Basic equations for 1D *N*-insulators and layer-by-layer

In the macroscopic derivation of E_d, E_d is constant except for surfaces and boundaries, which is confirmed in Fig. 2(d) and all the potential profiles studied. The thickness of surface layers or boundaries, in which the potential corresponding to macroscopic E_d deviates from atomic potential, is only $1 \sim 2$ unit-cell. In case of FE/vacuum, this deviation in 1-unit-cell thick regions is mainly due to work function (Appendix).

The other surface effects not included in the macroscopic derivation of E_d are buckling, i.e., inward dipole layer at the surface with ∼1 unit-cell thickness [40] and the atomic-scale variations of polarization P at the surface. However, these effects do not change the estimate of macroscopic E_d either, while we need to change the definition of the effective l_f as the thickness of the inner layers having a constant polarization P; Exemplarily in case of freestanding insulating 1D-FE, $\varepsilon_0 E_d + P = 0$ shows $E_d(z) = -P(z)/\varepsilon_0$, which means that E_d is unaffected by other locations as long as an end of FE is in an open vacuum. Consequently, we could confirm that the macroscopic formula of E_d agreed excellently with the *ab initio* E_d ($E_d^{ab\ initio}$) in all the a-few-nanometer-scale FEs studied here.

According to Sec. I, the correction to $P_{\rm S}^{\rm iso\text{-}bulk}$ is given by

$$Ps = Ps^{\rm iso-bulk} + (\varepsilon^{el} - 1)\varepsilon_0 E_d. \quad (1)$$

In Eq. (1), $\varepsilon_{\rm el}^{\rm Extra}$ is approximated by $\varepsilon^{\rm el}$ and E_d is given by *ab initio* calculation [Fig. 2(d)] or by

$$E_d = -\frac{P_S^{\rm iso-bulk} - P_I^{\rm iso-bulk}}{\varepsilon_0\left(\varepsilon^{el} + \frac{l_f}{l_I}\varepsilon_I^{el}\right)}, \tag{2a}$$

for a 1D system consisting of two insulators [Figs. 2(a) and 2(b)]. Equation (2a) is derived from Eq. (2b) for $N = 2$. Similarly, $P_I = P_I{}^{\rm iso\text{-}bulk} + (\varepsilon_I^{\rm el} - 1)\varepsilon_0 E_I$, where E_I is given by *ab initio* calculation [Fig. 2(d)] or $E_I = -E_d l_f/l_I$. The examples corresponding to Eq. (2a) are FE/vacuum, FE/insulator, and HH-TT domains [18]. For vacuum, $P_I{}^{\rm iso\text{-}bulk} = 0$ and $\varepsilon_I^{\rm el} = 1$, yielding $P_{\rm S} = P_{\rm S}{}^{\rm iso\text{-}bulk}\{1 - (\varepsilon^{\rm el} - 1)/(\varepsilon^{\rm el} + l_f/l_I)\}$.

Polarization and E_d of the kth layer in a 1D system consisting of N insulating layers are obtained by using Eq. (1): $P_j = P_j^{\rm iso\text{-}bulk} + (\varepsilon_j^{\rm el} - 1)\varepsilon_0 E_{dj}$ (P_j: corrected polarization at $j = 1 \sim N$), the continuity of flux $P_j^{\rm iso\text{-}bulk} + \varepsilon_j^{\rm el}\varepsilon_0 E_{dj} = P_{j+1}^{\rm iso\text{-}bulk} + \varepsilon_{j+1}^{\rm el}\varepsilon_0 E_{dj+1}$ ($j = 1 \sim N - 1$), and the continuity of potential for a periodic boundary condition $\Sigma_1^N l_j E_{dj} = 0$ with $E_{dN+1} = E_{d1}$, $\varepsilon_{N+1}^{\rm el} = \varepsilon_1^{el}$, and $P_{N+1}^{\rm iso\text{-}bulk} = P_1{}^{\rm iso\text{-}bulk}$. Here, P_j, $P_j^{\rm iso\text{-}bulk}$, $\varepsilon_j^{\rm el}$, E_{dj}, and l_j are the corrected (total) polarization, the polarization of an extracted bulk unit-cell, the permittivity of electrons, the depolarization field, and the thickness of the jth insulating layer. These relations yield

$$E_{dk} = -\frac{\sum_{j=1}^{N}\left\{\left(P_k^{\rm iso-bulk} - P_j^{\rm iso-bulk}\right)l_j/\varepsilon_j^{el}\right\}}{\varepsilon_k^{el}\varepsilon_0\ \sum_{j=1}^{N}\frac{l_j}{\varepsilon_j^{el}}}\ (k = 1 \sim N), \tag{2b}$$

which gives P_k by Eq. (1). The periodic boundary condition of electrostatic potential is clearly satisfied in short circuit 1D systems and also in open circuit 1D systems; For example, a freestanding FE in open vacuum is expressed by a periodic system [Fig. 2(a)] with $l_V = \infty$.

Equation (2b) for $N = 2$ yields Eq. (2a), by $E_{d1} = E_d$, $P_1{}^{\rm iso\text{-}bulk} = P_{\rm S}{}^{\rm iso\text{-}bulk}$, $\varepsilon_1^{\rm el} = \varepsilon^{\rm el}$, $l_1 = l_f$, $P_2{}^{\rm iso\text{-}bulk} = P_I{}^{\rm iso\text{-}bulk}$, $\varepsilon_2^{\rm el} = \varepsilon_I^{\rm el}$, and $l_2 = l_I$. The conducting layer, in which ϕ is constant, is considered as none and expressed by $\varepsilon_j^{\rm el} = \infty$ or $l_j = 0$; an example is an inner part of an electrode metal.

$P_j^{\rm iso\text{-}bulk}$ of some insulating layers such as the screening layers of metal electrodes is difficult to measure or define and usually expressed by $P_j = (\varepsilon_j - 1)\varepsilon_0 E_{dj}$. When a 1D system consists of such layers and the layers expressed by $P_j = P_j^{\rm iso\text{-}bulk} + (\varepsilon_j^{\rm el} - 1)\varepsilon_0 E_{dj}$ in the $k^{\rm th}$ insulating layer having $\varepsilon_k^{\rm el}$ is

$$E_{dk} = -\frac{\sum_{(\varepsilon_j^{el})}\left\{\left(P_k^{\rm iso-bulk} - P_j^{\rm iso-bulk}\right)l_j/\varepsilon_j^{el}\right\} + \sum_{(\varepsilon_j)}\left\{\frac{P_k^{\rm iso-bulk}l_j}{\varepsilon_j}\right\}}{\varepsilon_k^{el}\varepsilon_0\left(\sum_{(\varepsilon_j^{el})}\frac{l_j}{\varepsilon_j^{el}} + \sum_{(\varepsilon_j)}\frac{l_j}{\varepsilon_j}\right)}, \tag{2c}$$

where $\Sigma_{(\varepsilon_j^{\rm el})}$ and $\Sigma_{(\varepsilon_j)}$ are sum over the insulating layers expressed by $P_j = P_j^{\rm iso\text{-}bulk} + (\varepsilon_j^{\rm el} - 1)\varepsilon_0 E_{dj}$ and $P_j = (\varepsilon_j - 1)\varepsilon_0 E_{dj}$, respectively.

Unit-cell-scale layer-by-layer P_j and E_d (1D): Layer-by-layer polarization (corrected) P_j and E_d is obtained from ion positions in each unit-cell [Fig. 4(a)]. By regarding $P_j^{\rm iso\text{-}bulk}$ and l_j as $P_{\rm S}{}^{\rm iso\text{-}bulk}$ and c-lattice constant of each unit-cell, respectively, Eqs. (1) and (2b) [or (2c)] provide layer-layer $P_{\rm S}$ and E_d of each unit-cell [Fig. 4(b)]. In Eqs. (1), (2b), and (2c), $P_j^{\rm iso\text{-}bulk}$ and l_j can be approximated by average or typical $P_j^{\rm iso\text{-}bulk}$ and l_j. $\varepsilon_j^{\rm el}$ and ε_j can also be approximated as the constant for the same material with the same symmetry (Fig. 5). Because electronic peculiarity at the surface and metallic interface is not considered, this estimate may be inaccurate for the unit-cells at these locations.

B. Equations for typical situations

Freestanding FE and HH-TT domains: For freestanding FE in vacuum, Eq. (2b) yields, $E_d = -P_{\rm S}{}^{\rm iso\text{-}bulk}/\varepsilon_0\varepsilon^{\rm el}$ for $N = 2$, $E_{d1} = E_d$, $P_1{}^{\rm iso\text{-}bulk} = P_{\rm S}{}^{\rm iso\text{-}bulk}$, $\varepsilon_1^{\rm el} = \varepsilon^{\rm el}$, $P_2{}^{\rm iso\text{-}bulk} = 0$, $\varepsilon_2^{\rm el} = 1$, and $l_2 = \infty$. This formula $E_d = -P_{\rm S}{}^{\rm iso\text{-}bulk}/\varepsilon_0\varepsilon^{\rm el}$ is the same for periodic HH-TT domains as given by Eq. (2b) with $N = 2$, $E_{d1} = E_d$, $-P_2{}^{\rm iso\text{-}bulk} = P_1{}^{\rm iso\text{-}bulk} = P_{\rm S}{}^{\rm iso\text{-}bulk}$, $\varepsilon_2^{\rm el} = \varepsilon_1^{\rm el} = \varepsilon^{\rm el}$, and $l_2 = l_1 = l_f$.

Capacitors: Another common situation is a FE ($j = 2$) sandwiched with metals or semiconductors ($j = 1,\ 3$) in a short-circuited condition ($N = 3$). In this case, the effect of these metals and semiconductors appears only through a finite screening length. Equation (2c) is applicable with $P_j = (\varepsilon_j - 1)\varepsilon_0 E_{dj} (j = 1,\ 3)$ and $\Sigma_{(\varepsilon_j el)}$ in the numerator being zero. By setting $P_2{}^{\rm iso\text{-}bulk} = P_{\rm S}{}^{\rm iso\text{-}bulk}$ in $\Sigma_{(\varepsilon_j)}$ of the numerator, and $\varepsilon_2^{\rm el} = \varepsilon^{\rm el}$ and $l_2 = l_f$ in $\Sigma_{(\varepsilon_j el)}$ of the denominator,

$E_d = E_{d2} = -(P_{\rm S}{}^{\rm iso\text{-}bulk}l_1/\varepsilon_1 + P_{\rm S}{}^{\rm iso\text{-}bulk}l_3/\varepsilon_3)/\varepsilon^{\rm el}\varepsilon_0 (l_2/\varepsilon^{\rm el} + l_1/\varepsilon_1 + l_3/\varepsilon_3) = -P_{\rm S}{}^{\rm iso\text{-}bulk}/\varepsilon_0(\varepsilon^{\rm el} + \varepsilon_1 l_f/2l_1)$. The last equality is for identical electrode materials: $\varepsilon_1 = \varepsilon_3$ and $l_1 = l_3$, which is similar to a well-known formula [41]. This E_d yields $P_{\rm S} = \{1 - (\varepsilon^{\rm el} - 1)/(\varepsilon^{\rm el} + \varepsilon_1 l_f/2l_1)\}P_{\rm S}{}^{\rm iso\text{-}bulk}$.

Because $P_j^{\rm iso\text{-}bulk}$'s are accurately estimated from local ion positions by either the *ab initio* calculation or empirical formula [12] of an extracted unit-cell, these equations show that the corrected $P_{\rm S}$ (P_j) and $E_d(E_{dj})$ are obtainable from global ion positions. To obtain a macroscopic E_d (not layer by layer E_d), $P_{\rm S}{}^{\rm iso\text{-}bulk}$ and $P_I{}^{\rm iso\text{-}bulk}$ ($P_j^{\rm iso\text{-}bulk}$) can be approximated as constant except for the 1 unit-cell at the interface [Fig. 4(a)].

Metallic surface and domain boundaries: $E_d^{ab\ initio}$ is obtainable from *ab initio* potential profiles [Fig. 2(d)]. This estimation is possible, even when the surface and domain boundaries exhibit metallic energy band [16–18]. E_d is estimated experimentally as $E_d = Eg/el_f^{\rm insulate}$, where $l_f^{\rm insulate} \equiv l_f - 2l_{eh}$ and l_{eh} is the thickness of metallic layer and e is elementary charge. l_{eh} is 2 Å $\sim$ 10 Å. Therefore, the corrected $P_{\rm S}$ (P_j) and E_d (E_{dj}) are also obtainable from theoretical or experimental global ion positions.

When $l_f^{\rm insulate}$ of FE is too short, the *ab initio* potential profile of $I_{\rm adj}$ is used to calculate E_d through $E_d = -l_I E_I/l_f^{\rm insulate}$. Preferentially, the method of the estimation of Eg is same as that used for $P_{\rm S}{}^{\rm iso\text{-}bulk}$; When $P_{\rm S}{}^{\rm iso\text{-}bulk}$ is calculated *ab initio*

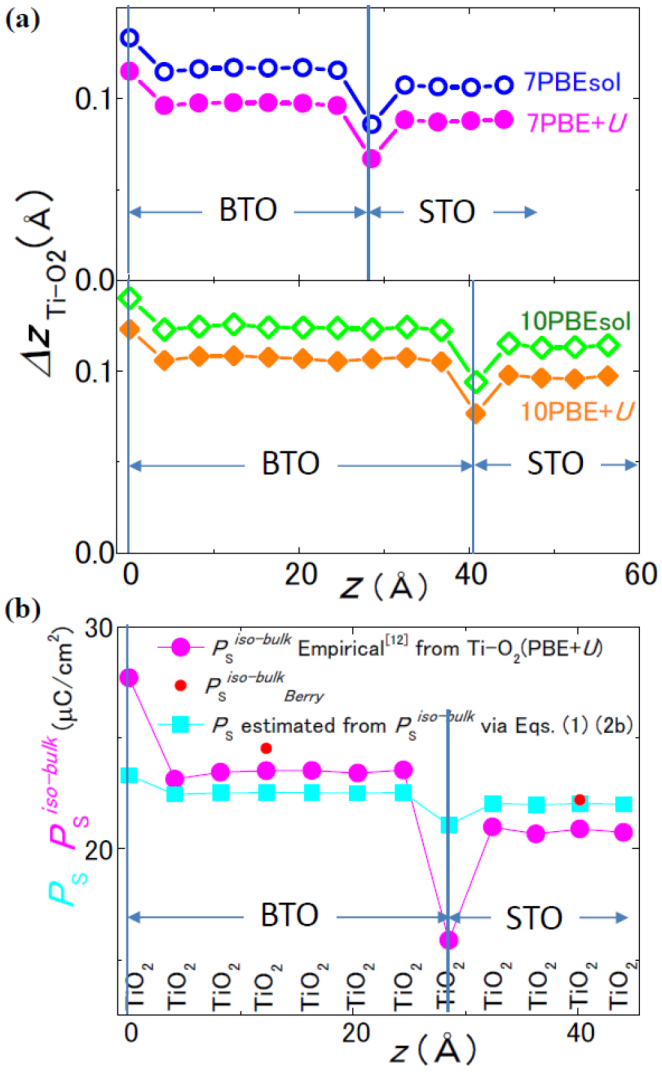

FIG. 4. (a) Layer-by-layer plot of the distance between Ti ion and O ion in TiO_2 plane along c-axis of n-unit-cell BTO/5-unit-cell STO superlattices ($n = 7,\ 10$). (b) $P_S^{\text{iso-bulk}}$ of each unit-cell having the ion positions shown by filled pink circles in (a) is represented by filled pink circles in (b). The corresponding $P_{S\ \text{Berry}}^{\text{iso-bulk}}$ is shown by a small red circle. The corrected polarization P_S is shown by filled light-blue squares.

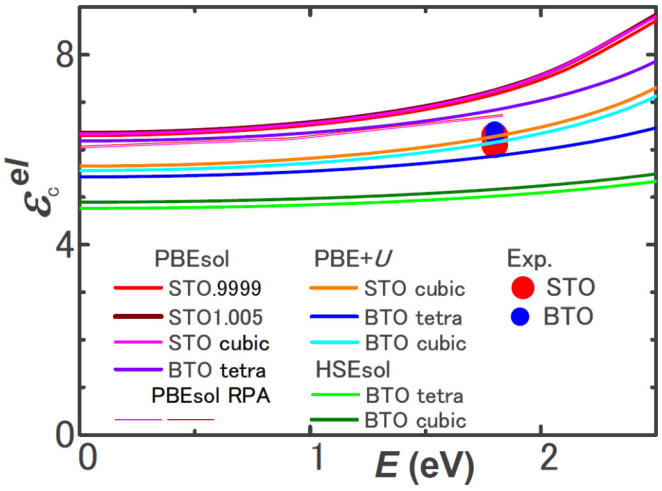

FIG. 5. Permittivity of electrons ε^{el} along c axis of STO1.005, STO.9999, cubic STO and BTO by *ab initio* calculations with PBEsol, PBE + U, and a hybrid functional HSEsol, while ε^{el} of STO1.005 is overlapped with that of cubic STO and almost invisible. Experimental optical ε^{el}'s [42] are also shown. In the PBEsol calculations of STO and STO.9999, the agreements with experiment were improved by RPA, which is shown by thin red and scarlet lines that are terminated near 1.8 eV. ε^{el} along a axis by each functional is very close to ε^{el} along c axis by each functional.

with PBEsol, Eg should be calculated with PBEsol, and when $P_S^{\text{iso-bulk}}$ is experimental, Eg should be experimental.

Defects and impurities: In the above procedures, Eqs. (2a)–(2c) and the *ab initio* calculations assume that the effects of defects and impurities are negligible. When the effects of defects and impurities are so evident that $E_d \approx 0$, the present method is unnecessary.

C. 3D P_S and E_d and representative value

Equations (1) and (2b) or (2c) can provide 3D distributions of P_j and E_d by changing $P_j^{\text{iso-bulk}}$, E_{dj}, and l_j to vector components $P^{\text{iso}}_{\alpha jxjyjz}$, $E_{d\alpha jxjyjz}$, $l_{\alpha jxjyjz}$, and $\varepsilon^{\text{el}}_{\alpha jxjyjz}$, respectively, where $\alpha = x, y, z$, and $j_x = 1 \sim N_x$, $j_y = 1 \sim N_y$, and $j_z = 1 \sim N_z$ denote the center of the uniform $P_S^{\text{iso-bulk}}$ block in Cartesian coordinates. In a unit-cell scale representation, j_x, j_y, and j_z denote the center position of a unit-cell, and $\varepsilon^{\text{el}}_{\alpha jxjyjz}$ can be approximated by a constant ε^{el} of a given polarization direction. For example, $P_{\alpha kxkykz} = P^{\text{iso}}_{\alpha kxkykz} + (\varepsilon^{\text{el}}_{\alpha kxkykz} - 1)\varepsilon_0 E_{d\alpha kxkykz}$ and $E_{dzkxkykz} = -\{\Sigma_{jz=1}^{Nz}(P^{\text{iso}}_{zkxkykz} - P^{\text{iso}}_{zkxkyjz})l_{zkxkyjz}/\varepsilon^{\text{el}}_{zkxkyjz}\}/\{\varepsilon^{\text{el}}_{zkxkykz}\varepsilon_0\Sigma_{jz=1}^{Nz} l_{zkxkyjz}/\varepsilon^{\text{el}}_{zkxkyjz}\}$ for the z component at the location center (k_x, k_y, k_z) by Eq. (2b).

In the application of the formula for 2D and 3D, all the boundaries should be consistently oriented; For example, the boundary between $P^{\text{iso}}_{\alpha jxjyjz}$ and $P^{\text{iso}}_{\alpha jxjyjz+1}$ should be perpendicular to z axis, and the boundary between $P^{\text{iso}}_{\alpha jxjyjz}$ and $P^{\text{iso}}_{\alpha jx+1jyjz}$ should be perpendicular to x axis. Therefore, the boundaries of 2D cases form steplike shapes. Practically, even for unit-cell scale P_j and E_d distribution, representative values of a large homogeneous block can approximate $P_{i\alpha jxjyjz}$, $E_{d\alpha jxjyjz}$, $l_{\alpha jxjyjz}$, and $\varepsilon^{\text{el}}_{\alpha jxjyjz}$ in the above sums, except for quantities of (k_x, k_y, k_z), i.e., the location to be calculated.

D. Value of $\varepsilon_{\text{el}}^{\text{Extra}}$

Ab initio and experimental electron's linear permittivity along c axis are shown in Fig. 5 [42]. The perturbation series expression of the electron's static permittivity is

$$\varepsilon^{el} = 1 + 2e^2\left\{\sum\frac{|x_{uo}|^2}{U_u - U_o} + eE\sum\sum\frac{x_{oi}x_{io}x_{oo}}{(U_i - U_o)^2} - \frac{x_{oi}x_{iu}x_{uo}}{(U_i - U_o)(U_u - U_o)} + e^2E^2..\right\}+, \quad (3)$$

where $x_{uo} = \int dr\Psi_u^* x\Psi_o$ and the subscripts o and $u(i)$ stands for occupied and unoccupied state, respectively, and U_o, U_i, and U_u are the corresponding Eigen-energies [43]. A typical minimum value of U_u–U_o (Eg) of good FEs is > 3 eV, while a typical energy of $ex_{uo}E$ is 0.8 meV

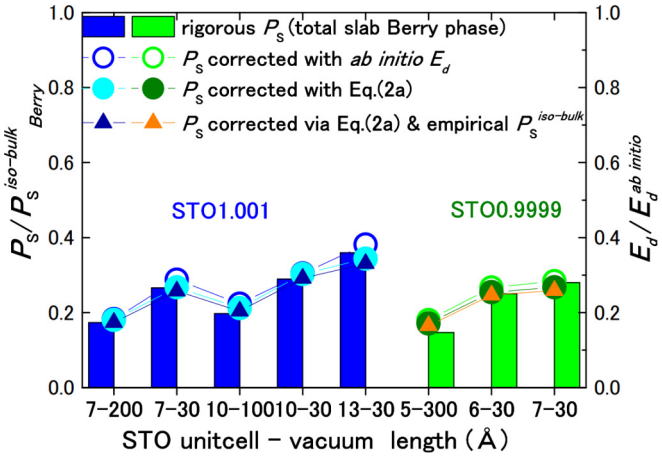

FIG. 6. Bars show the ratio of "Berry phase polarization P_S of a whole slab" to $P_S^{\text{iso-bulk}}{}_{\text{Berry}}$ [$P_S^{\text{iso-bulk}}{}_{\text{Berry}}$: Berry phase polarization of extracted bulk (Fig. 1(f), Table I)]. Open circles show the ratios of "P_S calculated by Eq. (1) using $E_d^{ab\ initio}$" to $P_S^{\text{iso-bulk}}{}_{\text{Berry}}$. Filled circles show the ratios of "P_S calculated by Eq. (1) using Eq. (2a)" to $P_S^{\text{iso-bulk}}{}_{\text{Berry}}$. Numbers n and m in n-m at the bottom represent the thicknesses of STO (in unit-cell) and vacuum (in Å), respectively. Triangles show the ratios of P_S to $P_S^{\text{iso-bulk}}$, where P_S is calculated by using Eq. (1), Eq. (2a), and $P_S^{\text{iso-bulk}}$ given by ion-position based empirical formula [12].

$(P_{el}^{\text{Exra}}/1\,\mu\text{C/cm}^2)(E_d/20\,\text{meV/Å})/N_e$, where $P_{el}^{\text{Exra}} = P_S - P_S^{\text{iso-bulk}}$ and N_e is the number of the contributing electrons per unit-cell. In case of ABO_3 type FEs, the electrons per unit-cell contributing to the lowest U_u–U_o are the O_{2p} valence electrons near the Fermi level E_F, and N_e is considered as 4. Therefore, $ex_{uo}E \ll U_u$–U_o, and the third- and higher-order terms are unimportant. This suggests that ε^{el} can be approximated as a constant even for a high electric field with a good accuracy. Therefore, we use the linear static electron permittivity obtained in Fig. 5, while similar examinations show that the nonlinearity is not negligible for the permittivity of ions.

The possible dependence of ε^{el} on u and, hence, P_S neglected, which is justified by Fig. 5 and the agreements of Eq. (2a) with $E_d^{ab\ initio}$ in Sec. IV; For example, ε^{el} of cubic BTO differs from ε^{el} of strained BTO only by 3%, where P_S's of these BTO's by HSEsol are 0 and 49 μC/cm^2, respectively [39]. Furthermore, Fig. 5 shows that $P_S^{\text{iso-bulk}}$ and, hence, u of STO1.005 and STO.9999 do not affect ε^{el}'s.

The exchange correlation functionals change the *ab initio* ε^{el}'s much more than the difference between STO and BTO; PBEsol yields the largest ε^{el}'s, and HSEsol yields the smallest ε^{el}. This difference is consistent with Eq. (3), because PBEsol yields the smallest Eg and HSEsol yields the largest Eg. The experimental ε^{el}'s are the closest to the ε^{el}'s calculated *ab initio* with PBE+U.

IV. ACCURACY OF THE METHOD

In this section, the total polarizations are normal to the surfaces and interfaces, and $\cos\theta = 1$.

FE/vacuum: All the eight kinds of STO/vacuum slabs labelled by the combination numbers in Fig. 6 exhibited the density of states (DOS) of insulators [Fig. 2(e)], and, therefore, Eq. (2a) with $P_I^{\text{iso-bulk}} = 0$ and $\varepsilon_l^{el} = 1$ was used. E_d ranges from 40 to 120 mV/Å, increasing with l_V/l_f and P_S. $\varepsilon^{el} = 6.2$ in Eqs. (1) and (2a) was a static limit of the electron permittivity calculated *ab initio* with PBEsol, because the *ab initio* calculations of other properties of STO/vacuum slabs were performed with PBEsol.

In Fig. 6, the ratios of rigorously calculated Berry phase P_S of the whole slab to $P_S^{\text{iso-bulk}}$ are shown by bars, where $P_S^{\text{iso-bulk}}$ is the *ab initio* spontaneous polarization $P_S^{\text{iso-bulk}}{}_{\text{Berry}}$ of an extracted bulk unit-cell consisting of 5 atoms similar to Table I. The ratios of P_S to $P_S^{\text{iso-bulk}}{}_{\text{Berry}}$ are shown by open and filled circles, where the open circles correspond to P_S by Eq. (1) using *ab initio* E_d ($E_d^{ab\ initio}$) and the filled circles correspond to P_S by Eq. (1) using Eq. (2a). Because the ion positions of all the unit-cells in each slab are exactly the same, $P_S^{\text{iso-bulk}}$'s of all the unit-cells are exactly the same.

Both P_S using $E_d^{ab\ initio}$ and P_S using E_d of Eq. (2a) agree excellently with rigorous ones. If one thinks that $P_S^{\text{iso-bulk}}$ is the total spontaneous polarization, which is conventional, the depolarization field $E_d^{\text{iso-bulk}}$ for FE/vacuum is $E_d^{\text{iso-bulk}} = -P_S^{\text{iso-bulk}}/\varepsilon_0(1 + l_f/l_I)$. Therefore, $E_d/E_d^{\text{iso-bulk}} = P_S/P_S^{\text{iso-bulk}}$, where $E_d = -P_S/\varepsilon_0(1 + l_f/l_I)$ is derived from Eqs. (1) and (2a) [30,44]. These ratios are shown in the right axis of Fig. 6. The appropriateness and importance of non-Born polarization P_{el}^{Exra} are evident in the small ratio of $P_S/P_S^{\text{iso-bulk}}$ and $E_d/E_d^{\text{iso-bulk}}$ as well as the excellent agreement of $P_S = P_S^{\text{iso-bulk}} + P_{el}^{\text{Exra}}$ with rigorously calculated P_S. These agreements for the whole range of $E_d = 40 \sim 120$ meV justify also the neglect of the nonlinearity of ε^{el} in Sec. III D.

Additionally, P_S's are calculated by Eqs. (1) and (2a) with $P_S^{\text{iso-bulk}}$'s given by $P_S^{\text{iso-bulk}} = 926\Delta z_{\text{Ti-O2}} - 0.05\,(\mu\text{C/cm}^2)$ [12], where $\Delta z_{\text{Ti-O2}}$ is the z component of the distance between Ti and O in TiO_2 plane ($z \parallel c$ axis) normalized by c-lattice constant of the unit-cell. The ratios of these P_S's to $P_S^{\text{iso-bulk}}{}_{\text{Berry}}$'s are shown in Fig. 6.

FE/insulator: All four BTO/STO slabs, labelled by the combination numbers in Fig. 7, exhibited DOS of states of insulators, and, hence, Eq. (2a) is used. E_d ranges from 15 to 23 mV/Å, decreasing with l_f. The accuracy of Eqs. (1) and (2a) was tested by the comparison of the Berry phase P_S of a whole slab with $P_S^{\text{slab}}{}_{\text{average}} \equiv (l_f P_S + l_I P_I)/(l_f + l_I)$, where P_S and P_I are calculated by Eqs. (1) and (2a). This test was performed using the 7-unit-cell BTO/5-unit-cell STO (PBE+U), and the ratio was 1.000.

The ratios of P_S to $P_S^{\text{iso-bulk}}$ are shown in Fig. 7(a), where P_S is calculated by both Eq. (1) using $E_d^{ab\ initio}$ and Eq. (1) using Eq. (2a). P_{el}^{Exra} changes $P_S^{\text{iso-bulk}}$ by 4% owing to small E_d. However, P_{el}^{Exra} changes E_d's substantially as seen Fig. 7(b). E_d's obtained through Eq. (2a) agree excellently with $E_d^{ab\ initio}$'s, while E_d given by $P_S^{\text{iso-bulk}}$, i.e., uncorrected spontaneous polarization is 6 ∼ 8 times larger than $E_d^{ab\ initio}$. These results prove the appropriateness and importance of P_{el}^{Exra}.

To test the practical estimations, E_d was calculated by Eq. (2a) using $P_S^{\text{iso-bulk}}$'s estimated by semi-empirical formulas $P_S^{\text{iso-bulk}}(\text{BTO}) = 977\Delta z_{\text{Ti-O2}} + 0.04\,(\mu\text{C/cm}^2)$ and $P_S^{\text{iso-bulk}}(\text{STO}) = 926\Delta z_{\text{Ti-O2}} - 0.05\,(\mu\text{C/cm}^2)$ [12]. The ratios of these E_d's to $E_d^{ab\ initio}$'s are shown as "by TiO_2" in Fig. 7(b).

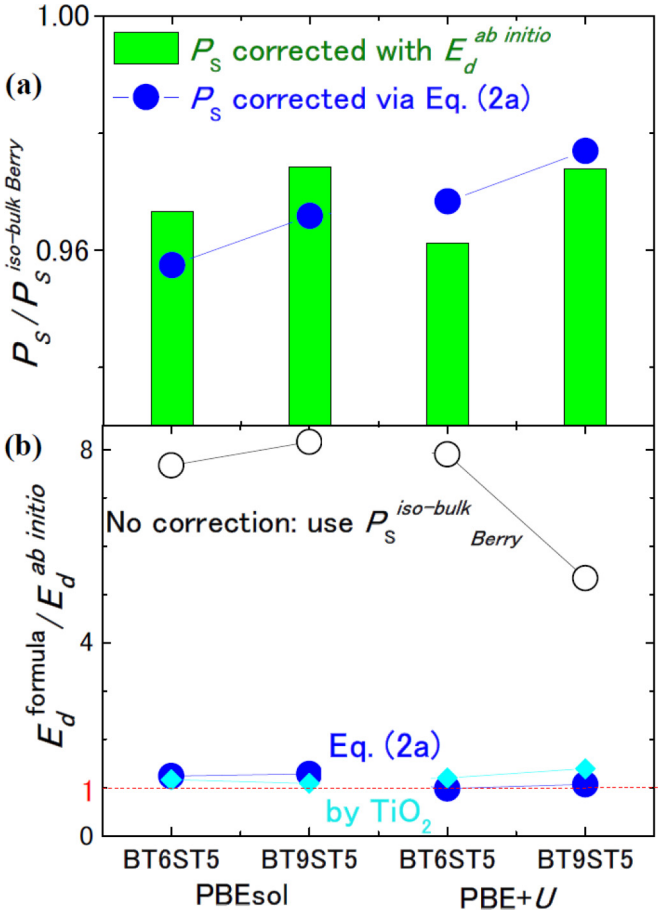

FIG. 7. (a) Bars show the ratio of "P_S calculated by Eq. (1)" using $E_d^{ab\ initio}$ to $P_S^{\text{iso-bulk}}{}_{\text{Berry}}$. Filled circles show the ratio of "P_S by Eq. (1) using Eq. (2a)" to $P_S^{\text{iso-bulk}}{}_{\text{Berry}}$. (b) Filled blue circles show the ratio of "E_d calculated with P_S and P_I (*corrected* by Eq. (2a))" to $E_d^{ab\ initio}$. Open black circles show the ratio of "E_d calculated with $P_S^{\text{iso-bulk}}{}_{\text{Berry}}$ and $P_I^{\text{iso-bulk}}{}_{\text{Berry}}$ (*uncorrected*)" to $E_d^{ab\ initio}$. The supercell geometry BTnSTm at the bottom represents the number of unit-cells in BTO and STO. Light blue diamonds show the ratios of "E_d by Eq. (2a)" to $E_d^{ab\ initio}$, where Eq. (2a) used $P_S^{\text{iso-bulk}}$ and $P_I^{\text{iso-bulk}}$ estimated by ion-position based empirical formula [12].

Additionally, the layer-by-layer P_S of each unit-cell was calculated by Eqs. (1) and (2b) in Fig. 4(b), where $\varepsilon_j^{\text{el}}$'s by PBE+$U$ were 5.36 (BTO) and 5.22 (STO) and l_j's were the distance between Ba or Sr atoms. For the layer-by-layer P_S, $P_j^{\text{iso-bulk}}$'s were estimated by the above semi-empirical formulas [12] using the layer-by-layer $\Delta z_{\text{Ti-O2}}$ in Fig. 4(a) and agreed with $P_S^{\text{iso-bulk}}{}_{\text{Berry}}$'s within 4% as seen in Fig. 4(b).

The layer-by-layer $P_S^{\text{iso-bulk}}$ varies substantially at the BTO-STO boundaries [Fig. 4(b)], yielding polarization charge $-\nabla \cdot P_S^{\text{iso-bulk}}$. The rescaled Born effective charges [23] yield the P_S variation similar to $P_S^{\text{iso-bulk}}$, because of the uniform scaling. However, electrons free from ions, i.e., $P_{\text{el}}^{\text{Exra}}$ are expected to smoothen the profile and reduce the variations at the BTO/STO boundaries, because these electrons are considered to screen electric field from $-\nabla \cdot P_S^{\text{iso-bulk}}$. This expectation is realized in P_S in Fig. 4(b), proving the appropriateness and usefulness of the non-Born-polarization $P_{\text{el}}^{\text{Exra}}$.

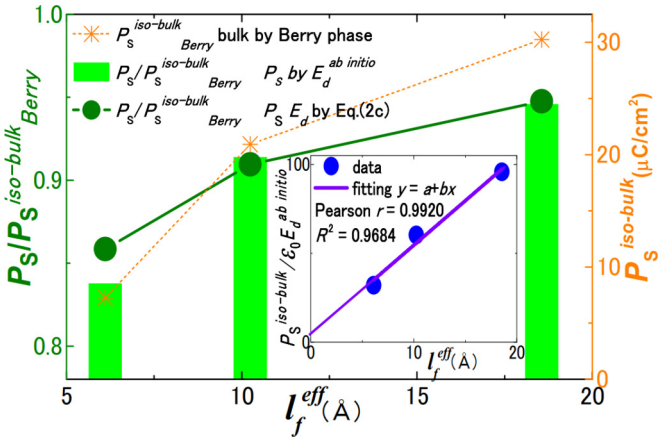

FIG. 8. Ratios of "P_S by Eq. (1)" and $E_d^{ab\ initio}$ to $P_S^{\text{iso-bulk}}{}_{\text{Berry}}$ shown by bars. Ratios of "P_S by Eqs. (1) and (2c)" to $P_S^{\text{iso-bulk}}{}_{\text{Berry}}$ are shown by filled dark-green circles. Asterisks show $P_S^{\text{iso-bulk}}{}_{\text{Berry}}$. Inset: Estimation of $\varepsilon_1/2l_1$ by liner fitting to $P_S^{\text{iso-bulk}}{}_{\text{Berry}}/\varepsilon_0 E_d$ vs. l_f^{eff} plot.

Short-circuited capacitor: The rigorous Berry phase calculation of P_S of these slabs are not possible. Additionally, because the thickness of the screening layer in short-circuited capacitors is less than 1 unit-cell, the polarization of an extracted unit-cell of electrodes $P_j^{\text{iso-bulk}}$ in Eq. (2b) was not estimated. Therefore, we used $E_d = -P_S^{\text{iso-bulk}}/\varepsilon_0(\varepsilon^{\text{el}} + \varepsilon_1 l_f/2l_1)$ given by Eq. (2c), for which only the spontaneous polarization of an extracted bulk unit-cell of FE $P_S^{\text{iso-bulk}}$ was required. In Fig. 8, $P_S^{\text{iso-bulk}}$ decreases as l_f^{eff} decreases, while E_d ranges from 26 to 39 mV/Å, reaching the maximum at $l_f^{\text{eff}} \approx 10$ Å.

In the inset of Fig. 8, $\varepsilon_1/2l_1$ was estimated as the inclination in $P_S^{\text{iso-bulk}}/\varepsilon_0 E_d^{ab\ initio}$ vs. l_f^{eff} plot and was 5.005 Å^{-1}, agreeing with the previous estimate [23]. P_S calculated by Eq. (1) with $E_d^{ab\ initio}$ is by 5% $\sim$ 15% lower than $P_S^{\text{iso-bulk}}$, showing the importance of $P_{\text{el}}^{\text{Exra}}$. These P_S's agree well with the P_S's calculated by Eq. (1) with Eq. (2c) $[-P_S^{\text{iso-bulk}}/\varepsilon_0(\varepsilon^{\text{el}} + \varepsilon_1 l_f/2l_1)]$, which is performed only with ion positions of a representative unit-cell and $\varepsilon_1/2l_1$. Additionally, E_d calculated by a macroscopic formula using P_S $[E_d = -P_S/\varepsilon_0(1 + l_f/l_I)$ derived from Eqs. (1) and (2a)] agreed with $E_d^{ab\ initio}$ better than those without correction, i.e., $P_S = P_S^{\text{iso-bulk}}$.

V. APPLICATION OF THE METHOD AND DOMAIN

The preceding results are for the depolarization field E_d, but the present method is similarly applicable for external field E_{ext}. For theoretical studies of insulting FEs under high fields such as MD and *ab initio* calculations [3–5,7–10,19,24,25], non-Born polarization $P_{\text{el}}^{\text{Exra}}$ is necessary. Here, insulting ideal FEs requires the absence of defects.

For experimental studies, the necessity of $P_{\text{el}}^{\text{Exra}}$ depends on sample and time-scale, on which the magnitude of E_d depends. However, in any case, E_d should be lower than the conventional estimates. As an example of a long time-scale case, we discuss *persisting* vortexlike P_S patterns, which are reported experimentally and attributed conventionally to E_d by the authors [3–5]. When these patterns are due to E_d [3–5], E_d at many locations should be high enough to change the

original P_S almost entirely and exists persistently in FE. The persistence of such high field can only be possible, when FE is unusually insulating and, hence, exceptionally stoichiometric. For such cases, the correction P_{el}^{Exra}, which reduces E_d but was missing so far, are necessary.

On the contrary, when FE in experiments [3–5] is not unusually insulating, the correction P_{el}^{Exra} is unnecessary. In this case, however, E_d cannot persist and, hence, cannot produce persisting vortexlike P_S patterns. That is, the primary origin of experimental vortexlike P_S patterns is not E_d, when FE is not unusually insulating.

A reference of insulativity of metal-oxide thin films is $LaAlO_3$/STO, which is exhaustively studied and exhibits defects and interdiffusion despite a state of art thin film growth technique [7,45]. The growth of stoichiometric metal-oxide thin film FE is more difficult than $LaAlO_3$/STO, because FEs contain highly volatile elements like Pb, Bi, Li, K, and Sb. Actually, scanning TEM experiments of strain-induced FE-STO at $LaAlO_3$/STO showed that E_d was almost zero, or of order of impurity ionization energies [8]. Therefore, the contribution of E_d to experimental vortexlike P_S patterns may be inessential, requiring other origins [26–28]. This inference may be consistent with the recent studies of Berezinskii-Kosterlitz-Thouless phase in 2D-FEs [46].

One of the origins is strain, which is considered as the origin of a/c (90°) domains of tetragonal FEs [26–28]. Natural half flux-closure domains consisting of a/c (90°) domains were reported by Hooton and Merz in 1955 [28], and Gregg [26] concluded that all the reported vortexlike P_S patterns were flux-closure domains that can reduce both strain and E_d. Indeed, all the vortexlike P_S patterns observed by TEM were not found at free surfaces but at the interface of FEs [3–5] that could provide enormous strain. The disappearance of domains on a metallic (La,Sr)MnO_3 layer [5] can be explained also by the reduced film quality of FE layer due to the (La,Sr)MnO_3 insertion and the decrease of strain. If these inferences are appropriate, vortexlike P_S patterns [3–5] can be nanometer-scale descriptions of classical a/c domains like Hooton and Merz that can reduce both strain and E_d [28].

VI. SUMMARY

For given ion positions or a unit-cell of insulating FEs and paraelectrics, the polarization $P_S^{iso\text{-}bulk}$ is estimated by standard methods such as *ab initio* calculations, Born effective charges, and empirical formula [2–5,7–10,11,12,15,19,24,25]. These estimations can be inadequate for the polarization under the depolarization field E_d, because E_d is determined by global boundary conditions and, hence, is absent in the bulk unit-cell extracted from the entire structure, e.g., slab; A unit-cell extracted from the total structure possesses the ion positions that corresponds to E_d, but E_d is absent in this unit-cell (Fig. 1, Table I). Consequently, unless electron polarization is completely associated with ion distortion u, a part of electron polarization, i.e., a part of atomic polarizability by E_d (P_{el}^{Exra}) is absent in these estimates, suggesting the inadequateness of polarization estimation based on local ion positions $P_S^{iso\text{-}bulk}$ (Sec. IV). Because P_{el}^{Exra} expresses the breakdown of the ion-position-polarization correspondence that is the basis of Born effective charges approaches (Appendix), we call P_{el}^{Exra} non-Born effective charge polarization.

For the polarization under field, we postulated P_{el}^{Exra} and proposed a method that calculated the total polarization $P_S = P_S^{iso\text{-}bulk} + P_{el}^{Exra}$ with $P_{el}^{Extra} = (\varepsilon_{el}^{Extra} - 1)\varepsilon_0 E$ or Eq. (1). This method worked, even when *ab initio* Berry phase calculation was not possible, and the correctness of the postulate and the high accuracy were demonstrated in Sec. IV, especially P_S and E_d of STO/vacuum and BTO/STO. In addition, the global consistency of $P_S^{iso\text{-}bulk}$ yielded formulas that calculated both P_S and E_d, using static electron permittivity, layer-thicknesses, and $P_S^{iso\text{-}bulk}$, which could also estimate 3D P_S and E_d in unit-cell-scale. Here, the unit-cell-scale layer-by-layer P_S could be also performed by algebra instead of *ab initio* Wannier approaches [23]. Because $P_S^{iso\text{-}bulk}$ is the conventionally estimated polarization, i.e., Born polarization, for which experimental ion positions can be used [11,12], these formulas enable the experimental estimation of P_S. The present method revealed a layer-by-layer P_S variation markedly flatter than that of conventional estimate $P_S^{iso\text{-}bulk}$, explaining successfully a small E_d and the absence of metallic layer formation by E_d [17,18]. The reduction of E_d is expected also for the situations of vortexlike domains. Because the order parameter of FE in GL theories is a total polarization [15], the incomplete entanglement of ion and electron polarization shown here implies limitation of GL framework of FE under high field.

ACKNOWLEDGMENTS

The discussions with P. Blöchel and the support from JSPS KAKENHI Grant No. JP19K21853 are acknowledged.

APPENDIX

Extracted unit-cell: $P_S^{iso\text{-}bulk}$ is the polarization of an extracted or copied unit-cell in which ion positions are exactly the same as those in the slab [Fig. 1(e)] and, hence, the ion distortion u due to E_d is fully contained [Fig. 1(f)] (Sec. I). This copied unit-cell can be called as a bulk with frozen ions as Table I shows; The ion positions and lattice of the copied unit-cell for $P_S^{iso\text{-}bulk}$ is the same as those of a unit-cell in the slab. In case of layer-by-layer estimation of $P_S^{iso\text{-}bulk}$, the extractions or copies similar to Table I are performed for all the unit-cells in the slab.

Born effective charges: Practical Born effective charges are not accurate as Berry phase calculations [20], because they are intended to estimate many different materials. However, Born effective charges can agree perfectly with Berry phase calculations, by incorporating u-dependence of Z^*, and other effects such as defects specific to the target FE. This possibility is confirmed by the perfect agreement of the curves expressed by a single u with Berry phase calculations in Fig. 9(a), where the polynomial for P_S includes the u-dependence of Z^*. The difference in P_S by the two method is invisible, whereas the difference in P_S by Berry phase calculations with PBEsol and TPSS [47] is evident. Additionally, Berry phase P_S of a bulk BTO having the experimental ion positions and lattice constants at 298 K ranged between 23 and 24 $\mu C/cm^2$ [39]. These results suggest that *ab initio* calculations are also approximations, although they are excellent. The quasilinearity

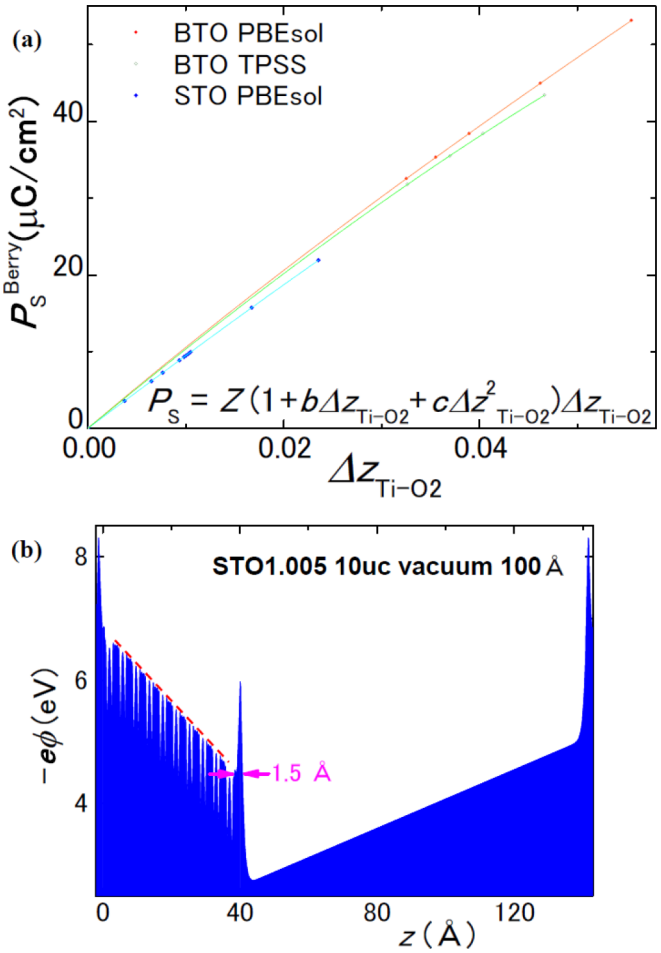

FIG. 9. (a) Relationship between Ti-O_2 distortion u (Δz_{Ti-O2}) and Berry phase P_S of BTO and STO calculated *ab initio* using specific exchange correlations extracted from Ref. [12], indicating that exact P_S can be obtained by Born effective charges. The curves by the polynomial in (a) are plotted by solid lines, where Z, b, and c are constants. (b) Example of the thickness of the surface layer of FE/vacuum and the estimation of $E_d^{ab\ initio}$ from the highest planar averaged ϕ by the *ab initio* calculation.

of the curves in Fig. 9 supports the practical accuracy of the standard Born effective charges $\Sigma Z^* u$ (Z^*: constant).

Therefore, both *ideal* Born effective charges and *ideal ab initio* calculations should yield the same $P_S^{\text{iso-bulk}}$, which is exact. Hence, because the physics or the spirit of Born effective charges is clear and describes the situation of $P_S^{\text{iso-bulk}}$, we call $P_S^{\text{iso-bulk}}$ Born polarization. Accordingly, the polarization not included in $P_S^{\text{iso-bulk}}$, i.e., P_{el}^{Exra} is called as non-Born effective charge polarization.

STO1.005, STO.9999: To achieve the insulativity of FE used in Berry phase calculations of P_S of a whole slab, STO1.005 and STO.9999 were chosen (Sec. II). For free-standing FEs and HH-TT domains, $E_d = -P_S^{\text{iso-bulk}}/\varepsilon_0\varepsilon^{\text{el}}$ by Eq. (2a), which yields $\phi_{\max} = l_f P_S^{\text{iso-bulk}}/\varepsilon_0\varepsilon^{\text{el}}$ ($\phi_{\max}$: maximum potential difference). Therefore, $l_f P_S^{\text{iso-bulk}}\varepsilon_0\varepsilon^{\text{el}} < Eg/e$ is required for insulativity [30]. This requires a very small $P_S^{\text{iso-bulk}}$, e.g., 3μC/cm^2 for l_f sufficiently long for the estimation of E_d by the method in Fig. 2(d). This is the reason for choosing STO1.005 and STO.9999. For example, even a 2-unit-cell-thick (∼8 Å) BTO in vacuum was metallic, when ion positions were fixed at those of a bulk BTO [48]. In case of STO1.005, 10-unit-cell-STO with $l_V = 100$ Å is marginally insulating, while 16-unit-cell-STO1.005 with $l_V = 30$ Å is metallic. In case of STO.9999, the critical l_f is reduced as in Fig. 2(e), owing to the increase of $P_S^{\text{iso-bulk}}$.

Additionally, the *ab initio* calculations by us and in literature (all ions relaxed) of 1D-FE/vacuum and 1D-HH-TT domains [10,16,19] show only two alternates: FE with metallic surface or paraelectric insulator, as predicted analytically [6,17]. Therefore, STO/vacuum was not relaxed to retain FE; Otherwise, it became paraelectric with $E_d = 0$.

No dipole correction: The dipole correction is used to imitate the experimental surfaces, for which $l_V = \infty$. The present target is not the FE surfaces ($l_V = \infty$) but FE/vacuum superlattices, because they are sufficient for the examinations of Eqs. (1)–(2c). Hence, the dipole correction was not applied.

Here, the change of P_S by the interactions between top and bottom surface is not a problem for the examinations of Eqs. (1)–(2c) by the comparison with *ab initio* results. These examinations were accurate, because we used *ab initio* $P_S^{\text{iso-bulk}}$, which contained the effect of the above interaction, in Eqs. (1)–(2c) and, hence, that effect was self-consistently included in both *ab initio* results and Eqs. (1)–(2c).

Surface layer and oblique case: Figure 9(b) shows that the thickness of the surface layer deviating macroscopic E_d, e.g., Eq. (2a) is ∼ 1.5 Å in FE/vacuum. For $\theta \neq 0$, Eq. (2b) changes to

$$E_{dk} = -\frac{\sum_{j=1}^{N}\left\{(P_k\cos\theta_k - P_j\cos\theta_j)l_j/\varepsilon_j^{el}\right\}}{\varepsilon_k^{el}\varepsilon_0\ \sum_{j=1}^{N} l_j/\varepsilon_j^{el}} \quad (k = 1 \sim N),$$

where θ_j is the angle of the polarization P_j to the 1D direction.

[1] C. Kittel, Rev. Mod. Phys. **21**, 541 (1949).
[2] P. Chen, M. P. Cosgriff, Q. Zhang, S. J. Callori, B. W. Adams, E. M. Dufresne, M. Dawber, and P. G. Evans, Phys. Rev. Lett. **110**, 047601 (2013).
[3] A. K. Yadav *et al.*, Nature **530**, 198 (2016).
[4] C.-L. Jia, K. W. Urban, M. Alexe, D. Hesse, and I. Vrejoiu, Science **331**, 1420 (2011).
[5] C. T. Nelson *et al.*, Nano Lett. **11**, 828 (2011).
[6] Y. Watanabe, J. Appl. Phys. **83**, 2179 (1998); Erratum: **84**, 3428 (1998).
[7] C.-P. Su, A. K. Singh, T. C. Wu, M. C. Chen, Y. C. Lai, W. L. Lee, G. Y. Guo, and M. W. Chu, Phys. Rev. Materials **3**, 075003 (2019).
[8] P. W. Lee *et al.*, Nat. Commun. **7**, 12773 (2016).

[9] S. Kouser, T. Nishimatsu, and U. V. Waghmare, Phys. Rev. B **88**, 064102 (2013); T. Nishimatsu, U. V. Waghmare, Y. Kawazoe, and D. Vanderbilt, *ibid.* **78**, 104104 (2008).

[10] N. Sai, C. J. Fennie, and A. A. Demkov, Phys. Rev. Lett. **102**, 107601 (2009).

[11] S. C. Abrahams, S. K. Kurtz, and P. B. Jamieson, Phys. Rev. **172**, 551 (1968).

[12] Y. Watanabe, Comput. Mater. Sci. **158**, 315 (2019).

[13] Ph. Ghosez, X. Gonze, Ph. Lambin, and J.-P. Michenaud, Phys. Rev. B **51**, 6765(R) (1995); X. Gonze and C. Lee, *ibid.* **55**, 10355 (1997); M. Posternak, R. Resta, and A. Baldereschi, *ibid.* **50**, 8911 (1994); J. D. Axe and W. A. Harrison, *Electronic Structure and the Properties of Solids* (Dover, New York, 1980).

[14] O. Diéguez, K. M. Rabe, and D. Vanderbilt, Phys. Rev. B **72**, 144101 (2005).

[15] A. F. Devonshire, Philos. Mag. **40**, 1040 (1949); especially p. 1056; **42**, 1065 (1951); especially p. 1067.

[16] S. Liu and R. E. Cohen, J. Phys.: Condens. Matter **29**, 244003 (2017).

[17] Y. Watanabe, Phys. Rev. B **57**, 789 (1998); Y. Watanabe and D. Sawamura, Jpn. J. Appl. Phys. **36**, 6162 (1997); Y. Watanabe, Ferroelectr. **333**, 57 (2006); Y. Watanabe and A. Masuda, Integr. Ferroelectr. **27**, 51 (1999).

[18] Y. Watanabe, M. Okano, and A. Masuda, Phys. Rev. Lett. **86**, 332 (2001).

[19] J. Sifuna, P. G.-Fernández, G. S. Manyali, G. Amolo, and J. Junquera, Phys. Rev. B **101**, 174114 (2020).

[20] C. Menéndez, D. Chu, and C. Cazorla, npj Comput. Mater. **6**, 76 (2020).

[21] J. Mitroy, M. S. Safronova and C. W Clark, and M. Atoji, J. Chem. Phys. **25**, 174 (1956).

[22] X. Wang and D. Vanderbilt, Phys. Rev. B **75**, 115116 (2007).

[23] M. Stengel, P. Aguado-Puente, N. A. Spaldin, and J. Junquera, Phys. Rev. B **83**, 235112 (2011); Born effective charge rescaling Eq. (33) or Eq. (A7) is described in the Appendix.

[24] I. I. Naumov, L. Bellaiche, and H. Fu, Nature **432**, 737 (2004).

[25] Y.-H. Shin, I. Grinberg, I-W. Chen, and A. M. Rappe, Nature **449**, 881 (2007).

[26] J. M. Gregg, Ferroelectr. **433**, 74 (2012).

[27] S. K. Streiffer *et al.*, J. Appl. Phys. **83**, 2742 (1998).

[28] J. A. Hooton and W. J. Merz, Phys. Rev. **98**, 409 (1955).

[29] Y. Watanabe, Phys. Rev. B **99**, 064107 (2019).

[30] Y. Watanabe (unpublished).

[31] G. Kresse and J. Hafner, Phys. Rev. B **47**, 558 (1993); G. Kresse and J. Furthmüller, Comput. Mater. Sci. **6**, 15 (1996); Phys. Rev. B **54**, 11169 (1996); G. Kresse and D. Joubert, *ibid.* **59**, 1758 (1999); M. Hutchinson and M. Widom, Comput. Phys. Commun. **183**, 1422 (2012); M. Hacene, A. A. Sedrakian, X. Rozanska, D. Klahr, T. Guignon, and P. F. Lessard, J. Comput. Chem. **33**, 2581 (2012).

[32] P. E. Blöchl, Phys. Rev. B **50**, 17953 (1994).

[33] J. P. Perdew, A. Ruzsinszky, G. I. Csonka, O. A. Vydrov, G. E. Scuseria, L. A. Constantin, X. Zhou, and K. Burke, Phys. Rev. Lett. **100**, 136406 (2008).

[34] H. J. Monkhorst and J. D. Pack, Phys. Rev. B **13**, 5188 (1976).

[35] R. Resta, Rev. Mod. Phys. **66**, 899 (1994); R. D. King-Smith and D. Vanderbilt, Phys. Rev. B **47**, 1651 (1993).

[36] J. P. Perdew, K. Burke, and M. Ernzerhof, Phys. Rev. Lett. **77**, 3865 (1996).

[37] A. I. Liechtenstein, V. I. Anisimov, and J. Zaanen, Phys. Rev. B **52**, R5467 (1995).

[38] J. Heyd, G. E. Scuseria, M. Ernzerhof, J. Chem. Phys. **118**, 8207 (2003); L. Schimka, J. Harl, and G. Kresse, *ibid.* **134**, 024116 (2011).

[39] Y. Watanabe, J. Chem. Phys. **148**, 194702 (2018).

[40] 5. N. Bickel, G. Schmidt, K. Heinz, and K. Müller, Phys. Rev. Lett. **62**, 2009 (1989).

[41] R. R. Mehta, B. D. Silverman, and J. T. Jacobs, J. Appl. Phys. **44**, 3379 (1973).

[42] M. Cardona, Phys. Rev. **140**, A651 (1963); W. L. Bond and A. R. Johnston, J. Appl. Phys. **42**, 3501 (1971).

[43] J. J. Sakurai, Title (Addison Wesley, Redwood, 1985), Chap. 5.1, p. 296; L. I. Shiff, *Quantum Mechanics,* 3rd ed. (McGraw Hill, New York, 1968), Chap. 8, Sec. 33, p. 264; A. S. Kompaneyets and J. M. Ziman, *Principles of the Theory of Solids,* 2nd ed. (Cambridge University Press, Cambridge, UK, 1972), Chap. V, Sec. 5.6.

[44] Y. Watanabe, Ferroelectr. **461**, 38 (2014).

[45] S. A. Pauli *et al.*, Phys. Rev. Lett. **106**, 036101 (2011); Y. Li, X. Wei, and J. Yu, J. Appl. Phys. **127**, 205302 (2020).

[46] C. Xu, Y. Nahas, S. Prokhorenko, H. Xiang, and L. Bellaiche, Phys. Rev. B **101**, 241402(R) (2020); J. W. Villanova, P. Kumar, and S. Barraza-Lopez, *ibid.* **101**, 184101 (2020).

[47] J. Tao, J. P. Perdew, V. N. Staroverov, and G. E. Scuseria, Phys. Rev. Lett. **91**, 146401 (2003).

[48] Y. Watanabe, Ferroelectr. **556**, 29 (2020).